Entropy-Driven Clustering in Tetrahedrally Bonded Multinary Materials

Paweł Zawadzki,[*] Andriy Zakutayev, and Stephan Lany

National Renewable Energy Laboratory, Golden, Colorado 80401, USA
(Received 10 September 2014; revised manuscript received 8 January 2015; published 19 March 2015)

Compositional inhomogeneities in multielemental materials typically form due to lowering of the energy relative to the homogeneous phase. Here, we demonstrate an entropy-driven mechanism in the zinc-blende derived cation-substituted multinary compounds Cu_2SnS_3 (CTS) and Cu_2ZnSnS_4 (CZTS). Using a motif-based model Hamiltonian and Monte Carlo simulations, we find that disorder leads to a redistribution of the structural motifs in such a way to create cation clustering. The associated formation of (sub-) nanometer-scale compositional inhomogeneities can cause potential fluctuations with detrimental consequences for photovoltaic applications.

I. INTRODUCTION

Multinary materials are advantageous for many applications because they provide wide compositional parameter space in which material properties can be tuned. The increased compositional complexity, however, has an important side effect, namely, the increased propensity for compositional fluctuations that preserve the underlying structure of the material and therefore are difficult to detect and characterize experimentally [1,2]. In solar absorbers, such disorder effects can be particularly problematic, because compositional inhomogeneities lead to spatial band-gap and electrostatic potential fluctuations. Furthermore, such fluctuations can lead to localization of photogenerated charge carriers (formation of fluctuons [3,4]) or even to charge trapping in the band tails. The resulting decrease of the minority carrier mobility and lifetime, as well as increased recombination losses, are detrimental to the performance of photovoltaic (PV) devices [5].

Indeed, cation disorder [6–13] and formation of compositional inhomogeneities [14–17] are implicated as possible reasons for low open-circuit voltage limiting the performance of Cu_2ZnSnS_4 (CZTS) solar cells [18]. Understanding the origin and the consequences of atomic disorder is therefore critical for the design of next-generation PV devices based on Cu_2SnS_3 (CTS) and CZTS considered here, or on other multinary compounds discussed for photovoltaics, such as $ZnSnN_2$ [19] or Cu_3SbS_4 [20].

Here, we use a motif-based model Hamiltonian and Monte Carlo simulations to show that in both CTS and CZTS, cation disorder leads to formation of compositional inhomogeneities due to entropy-driven clustering of S-centered tetrahedral motifs of the underlying zinc-blende lattice. The ground-state structure of CTS is built from two different motifs, and disorder leads to the clustering of these

motifs. CZTS, on the other hand, is a single-motif phase in the kesterite structure. However, the decomposition of the ground-state motif is energetically inexpensive and leads to a phase transition into a multimotif phase at critical temperature $T_c = 470$ K. These findings suggest that such ternary or multinary compounds are preferable, in which the ground state is a single-motif structure and the formation of other motifs is energetically unfavorable.

II. CATION COORDINATION AND THE OCTET RULE IN CTS AND CZTS

The structures of CTS and CZTS can be derived by appropriate ordering of Cu, Sn, and Zn atoms on cationic sites of the zinc-blende ZnS lattice [21]. In both materials, the local cation ordering is constrained by the so-called octet rule. The octet rule, in an ionic picture, states that configurations with eight valence electrons per anion are energetically favorable. Since the crystal structures of CTS and CZTS are derived from an underlying zinc-blende lattice, both cations and anions are four-fold coordinated. From the point of view of the anion (S), there are 15 possible different coordinations, i.e., the S-$Cu_iSn_jZn_{\{4-i-j\}}$ motifs, where $0 \leq i \leq 4$, $0 \leq j \leq 4 - i$. Taking into account that the cation charge is shared by four anions, the number of electrons in the valence shell of a given S atom at the center of a motif is $N_v = 8 + (2j - i)/4$.

Applying the octet rule locally to S anions in CZTS, one finds that the S-Cu_2SnZn ($N_v = 8$) motif should describe the preferred cation coordination of S. Indeed, this motif is the building block of the ground-state kesterite structure (space group $I4$) of CZTS, and also of the stannite structure (space group $I\bar{4}2m$), which is a low-energy structure [17,22] with a different arrangement of the S-Cu_2ZnSn motifs. In CTS, on the other hand, the octet rule cannot be exactly satisfied by any single motif, and the ground-state monoclinic CTS (space group Cc) is built from motifs that offer the smallest deviation from the rule,

[*]Corresponding author.
pawel.zawadzki@nrel.gov

i.e., S-Cu_2Sn_2 ($N_v = 8.5$) and S-Cu_3Sn ($N_v = 7.75$). Thus, the octet rule describes not only the overall composition, but also the local cation coordination of the anions in the ordered ground-state crystal structures of CTS and CZTS.

At higher temperatures, both CZTS and CTS exhibit cation disorder. With increasing temperature, monoclinic CTS first assumes a tetragonal phase, with two-thirds of Cu sites mixed with Sn sites (space group $I\bar{4}m$) and then a cubic phase at ~350 °C [23–25] with all cationic sites mixed (space group $F\bar{4}3m$). CZTS transforms from the tetragonal into a cubic phase at ~1100 K [26]. However, x-ray [8,9,13] and neutron [13] diffraction, Raman [6,7] and photoluminescence [7,12] spectroscopies, or nuclear-magnetic-resonance measurements [12] show that already tetragonal CZTS exhibits a high degree of cation disorder, mostly due to mixing between Cu and Zn sites.

III. MODEL AND METHODS

A. Energy expansion in local motifs

In this work, we use a motif-based model, inspired by the local octet rule, to obtain an expansion of the energy related to the cation arrangement. This model Hamiltonian allows us to perform Monte Carlo simulations to obtain atomistic representations of disordered structures of CTS and CZTS, and serves as a basis to study the consequences for application as solar-absorber materials in photovoltaics. Within the motif-based model, the formation energy is approximated as a linear function of the composition vector, whose elements $n_{(i,j)}$ count the number of sulfur-based S-$Cu_iSn_jZn_{4-i-j}$ tetrahedral motifs,

$$\Delta_f E = 2 \sum_{(i,j)} n_{(i,j)} e(i,j). \tag{1}$$

The expansion parameters $e(i,j)$, listed in Fig. 1, are determined by a least-squares fit to the formation energies of a test set of various Cu, Sn, and Zn configurations on a cationic sublattice of the zinc-blende structure (for details, see Sec. III B). Despite its simplicity, the expansion, Eq. (1), results in a remarkably accurate description of the test-set energies with an out-of-sample error of 4 meV/atom.

The emphasis on local coordination allows for an interpretation in terms of preferred local chemistries, and the expansion parameters $e(i,j)$ have a clear physical meaning in that they describe the formation energy of zinc-blende phases built entirely from the respective motifs. The Hamiltonian does not include long-range interactions; therefore, different arrangements of the same types and numbers of motifs are degenerate in energy. The difference between the mean formation energy of disordered phases and the formation energy of the ground-state ordered structure, however, is small and equals 9 meV/atom and 5 meV/atom for CTS and CZTS, respectively. Alternatively, the disorder could be described by cluster expansion techniques [27], but the mixing of three non-isovalent elements on the cation sublattice of CZTS would require a rather involved ternary cluster expansion [28]. Using the motif-based Hamiltonian, Eq. (1), we perform canonical (NVT) ensemble Metropolis Monte Carlo simulations of CZTS and CTS with randomly initialized cation configurations on the cationic sublattice of the zinc-blende structure. The samples are first heated to 1773 K, then annealed to 73 K in about 10^7 steps.

B. Computational methods

The parameters of the model Hamiltonian are fitted to formation energies calculated with density function theory (DFT) with an on-site Coulomb energy [29] $U = 5$ eV applied to Cu(d) states using the Perdew-Burke-Ernzerhof [30] exchange correlation functional and the VASP code [31]. The training set consists of 160 random $Cu_xSn_yZn_{1-x-y}S$ zinc-blende structures that preserve the nominal oxidation states of atoms in CZTS—that is, +1 of Cu, +4 of Sn, and +2 of Zn. The volumes, cell shapes, and ionic positions of each structure are optimized and the formation energies are calculated using fitted reference atomic energies [32]. To calculate the out-of-sample mean absolute error, we use the cross-validation [33] with five iterations and random train-test split of 2:1. The mean absolute error is 4 meV/atom.

Monte Carlo simulations are performed using 384 (24 samples) and 1200 (24 samples) atom cells of CTS and CZTS, respectively. The cation distribution in each sample is randomly initialized. To obtain more accurate order-disorder phase transition in CZTS, the S-Cu_3Sn and S-Cu_2SnZn parameters of the model Hamiltonian are refitted to DFT formation energies of 25 (300 atom) structures generated with the Monte Carlo simulation at temperatures spanning the phase-transition region. This refitting allows us to reduce the cross-validation error to 1 meV/atom.

IV. RESULTS AND DISCUSSION

A. Cation disorder and clustering in CTS

We first examine cation disorder in the simpler case of the ternary CTS before addressing disorder in the more complex quaternary CZTS. An initial CTS structure with randomly distributed cations contains all five possible

j\\i	0	1	2	3	4
0	−1.083	−0.914	−0.679	−0.404	−0.238
1	−0.880	−0.790	−0.663	−0.492	
2	−0.565	−0.563	−0.463		
3	−0.379	−0.254			
4	−0.026				

S-$CuSnZn_2$
S-Cu_2SnZn
S-Cu_3Sn
S-Cu_2Sn_2

FIG. 1. Parameters $e(i,j)$ in eV/atom of the model Hamiltonian, Eq. (1).

S-Cu_iSn_{4-i} motifs, where $i \in \{0, ..., 4\}$. The equilibration at 1773 K removes the majority of S-Cu_4, S-$CuSn_3$, and S-Sn_4 motifs and the structure is built almost entirely from S-Cu_3Sn and S-Cu_2Sn_2 motifs, i.e., motifs that constitute the ordered CTS. This outcome of the MC simulation is a result of the energetically unfavorable disproportionation pathways of the S-Cu_3Sn and S-Cu_2Sn_2 motifs: The lowest-energy decomposition reactions are, 2 S-$Cu_2Sn_2 \rightarrow$ S-Cu_3Sn + S-$CuSn_3$ and 2 S-$Cu_3Sn \rightarrow$ S-Cu_4 + S-Cu_2Sn_2, which require 360 meV and 570 meV, respectively. These energies are larger than 5 k_BT at the typical deposition temperature of 700 K, implying an equilibrium concentration of these motifs in the subpercent range.

Figures 2(a) and 2(b) compare the distribution of S-Cu_2Sn_2 motifs between the ordered and disordered CTS as calculated by the MC simulations. In its monoclinic ground-state structure, CTS is built from the S-Cu_2Sn_2 and S-Cu_3Sn motifs that are uniformly distributed [cf. Fig. 2(a)]. In the disordered, cubic CTS structure obtained from the Monte Carlo simulations, however, the S-Cu_2Sn_2 motifs form nanometer-scale clusters. This observation may be surprising at first because the ordered and disordered CTS structures have the same energy within the Hamiltonian, Eq. (1), since they are built from the same types and numbers of motifs. The change in the Helmholtz free energy, $\Delta A = \Delta E - T\Delta S$, the minimum of which defines the equilibrium of the NVT ensemble, is thus only due to entropy change: $\Delta A = -T\Delta S$. On the other hand, entropy-driven disorder is usually associated with random and homogeneous distributions but not with clustering. However, since the tetrahedra are connected [cf. Fig. 3(a)], the different motifs cannot be formed and arranged independently from each other. Thus, the observed clustering indicates the presence of attractive entropic forces [34] that reflect these constraints.

In order to understand the origin of such entropic forces, and to rationalize the results of the MC simulations, we are now considering a small cluster where the different cation arrangements can be enumerated. Figure 3(a) illustrates the assemblage of motifs composed of a central S-Cu_2Sn_2 motif and its first coordination shell consisting of x S-Cu_2Sn_2 and $12 - x$ S-Cu_3Sn motifs [cf. Fig. 3(a)]. Note that we impose the constraint that only these two motifs are present, since the formation of other motifs is associated with a considerable energy cost (cf. Fig. 1). Because the energy is linear in the concentration of motifs, all the configurations of Cu and Sn atoms in the assemblage (microstates) that result in a given x (macrostate) have the same energy. The entropy takes the microcanonical form $S(x) = k_B \ln W(x)$, where $W(x)$ is the number of possible configurations of Cu and Sn atoms that lead to a given coordination number x. [The term "coordination number" is used in the following to denote by how many motifs of the same type a certain motif is surrounded; cf. Fig. 3(a).] The entropy $S(x)$ for the S-Cu_2Sn_2-centered clusters is shown in
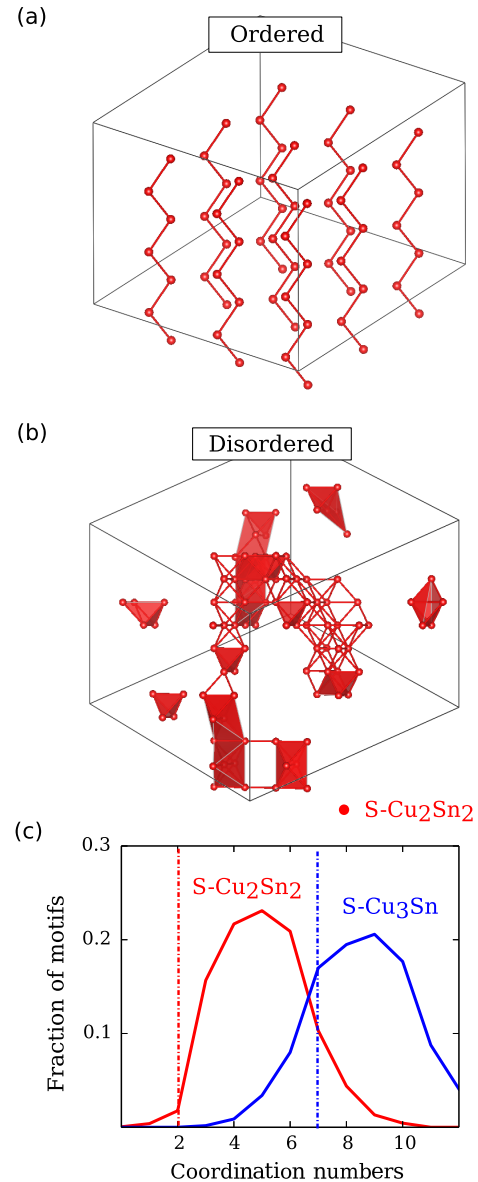

FIG. 2. Ordering of the S-centered motifs in Cu_2SnS_3 (CTS). Sulfur atoms in the center of a S-Cu_2Sn_2 motif are shown in red. All remaining S atoms are the center of a Cu_3Sn motif and are omitted for clarity. (a) Ordered CTS in the monoclinic ground-state crystal structure. (b) A disordered structure of CTS obtained from Monte Carlo simulations. (c) The distribution of coordination numbers for S-Cu_2Sn_2 (red) and S-Cu_3Sn (blue) motifs in the monoclinic ground state (dash-dotted lines) and in the disordered state (solid lines).

Fig. 3(b) (red solid line). The entropy takes the maximum at $x = 6.7$, i.e., for $x < 6.7$ ($x > 6.7$) there is an attractive (repulsive) entropic force $F(x) = TdS/dx$ between S-Cu_2Sn_2 motifs (red dashed line). A similar analysis is made for the S-Cu_3Sn motif being surrounded by y Cu_3Sn and $12 - y$ Cu_2Sn_2 motifs. In this case, we find that the entropic forces are positive for $y < 6.3$ and negative for $y > 6.3$ [cf. blue lines in Fig. 3(b)]. In ordered CTS, the S-Cu_2Sn_2 and S-Cu_3Sn motifs are coordinated by $x = 2$
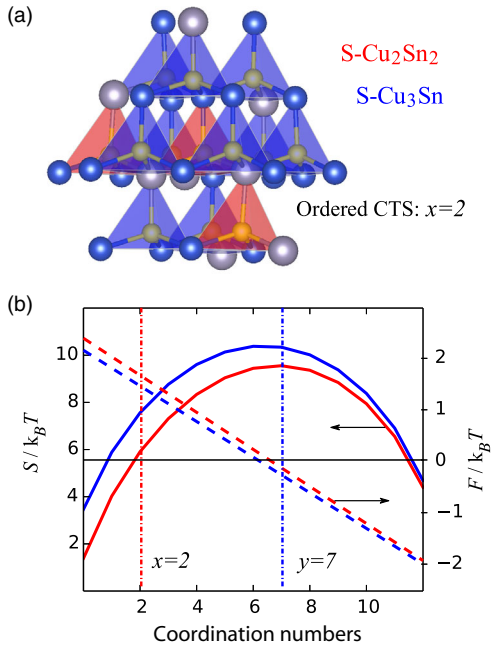
FIG. 3.   Clustering of motifs in Cu_2SnS_3 (CTS). (a) An assemblage of 13 motifs composed of a central $S\text{-}Cu_2Sn_2$ motif surrounded by $x = 2$ $S\text{-}Cu_2Sn_2$ and $12 - x = 10$ $S\text{-}Cu_3Sn$ motifs in the first coordination shell. (b) Entropy (solid line) and entropic force (dashed line) obtained from enumeration of cation arrangements in the 13-motif cluster. The entropies and forces are shown for $S\text{-}Cu_2Sn_2$ motifs (red) and $S\text{-}Cu_3Sn$ motif (blue) as a function of x and y, i.e., the respective coordination numbers (number of surrounding motifs of the same type). In ordered monoclinic CTS, the $S\text{-}Cu_2Sn_2$ and $S\text{-}Cu_3Sn$ motifs have coordination numbers $x = 2$ and $y = 7$ (dash-dotted lines), respecive.

and $y = 7$. Thus, this statistical analysis suggests that the $S\text{-}Cu_2Sn_2$ and $S\text{-}Cu_3Sn$ motifs in ordered CTS experience strong attractive and weak repulsive entropic forces, respectively.

The statistical enumeration based on the small cluster (Fig. 3) neglects, of course, interconnections between motifs in a more extended system, where the coordinations of the $S\text{-}Cu_2Sn_2$ and $S\text{-}Cu_3Sn$ motifs cannot be varied independently. However, the presence of entropic forces is clearly reflected in the distribution of coordination numbers in the extended structures obtained from the Monte Carlo supercell simulations of disordered CTS, shown in Fig. 2(c). The coordination number of $S\text{-}Cu_2Sn_2$ motifs increases from $x = 2$ in the ordered ground-state structure to an average coordination of $\bar{x} = 5.0$ in the disordered state, reflecting the clustering of $S\text{-}Cu_2Sn_2$ motifs in the disordered structure [cf. Fig. 2(b)]. The clustering of $S\text{-}Cu_2Sn_2$ motifs, in turn, also necessitates an increased degree of clustering of the $S\text{-}Cu_3Sn$ motifs, even though the statistical enumeration above suggests a weak repulsive entropic force (i.e., anticlustering). Consequently, the coordination of the $S\text{-}Cu_3Sn$ motif increases slightly, from $y = 7$ in the ordered state to

$\bar{y} = 8.5$ in disordered CTS. It is notable that the disorder-induced clustering of motifs in CTS is only weakly dependent on temperature. Since the energy difference between ordered and disordered CTS is small (zero within the model Hamiltonian), the clustering is mainly a consequence of the geometric constraints on the possible cation arrangements due to the requirement of avoiding the formation of high-energy motifs other than $S\text{-}Cu_2Sn_2$ or Cu_3Sn.

B. Cation disorder and clustering in CZTS

Let us now analyze disorder in the more complex case of the quaternary CZTS. In contrast to CTS, CZTS is built from only one motif, i.e., $S\text{-}Cu_2ZnSn$, in its ground-state structure at 0 K, but increasing the temperature leads to the formation of new motifs. The main pathway for the creation of new motifs is the disproportionation of $S\text{-}Cu_2SnZn$ into $S\text{-}Cu_3Sn$ and $S\text{-}CuSnZn_2$ motifs, which requires only 88 meV (cf. Fig. 1) and causes a second-order phase transition from a single-motif to a multimotif phase with $T_c = 470$ K (cf. Fig. 4). We note that this finding is consistent with experimental observations: A second-order phase transition in CZTS with $T_c = 533$ K is observed by monitoring the change in Raman signal due to S-related local vibrational modes [6]. Neutron-diffraction measurements show that the position of the S atom changes around $T_c \sim 500$ K, suggesting that the local coordination of the S atom changes [26]. Also, the formation of $S\text{-}Cu_3Sn$ and $S\text{-}CuSnZn_2$ motifs out of $S\text{-}Cu_2SnZn$ motifs is a direct consequence of the mixing between Cu and Zn sites [35], which is deduced from neutron scattering [13], synchrotron x-ray diffraction [8,9,13] experiments and discussed in the literature in the framework of the point-defect model [36].

The Monte Carlo simulations show that when the $S\text{-}Cu_3Sn$ and $S\text{-}CuSnZn_2$ form in CZTS with increasing temperature, they cluster, similarly to the case of CTS discussed above. For instance, at 2% concentration, corresponding to ~420 K in Fig. 5(a), the $S\text{-}Cu_3Sn$ motifs
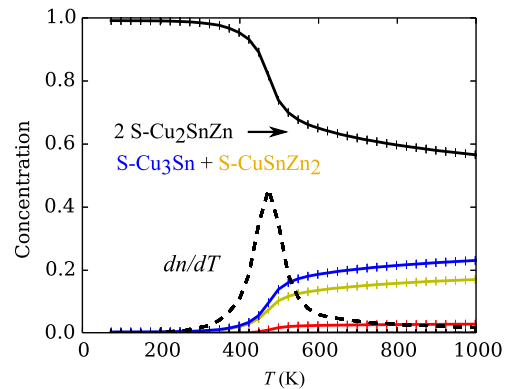

FIG. 4.   Phase transition in Cu_2ZnSnS_4 (CZTS). Concentration of $S\text{-}Cu_2SnZn$ (black solid line), $S\text{-}Cu_3Sn$ (blue solid line), $S\text{-}CuSnZn_2$ (yellow solid line), and $S\text{-}CuSn_3$ (red solid line) motifs as a function of temperature. The black dashed line shows the first derivative of the concentration of $S\text{-}Cu_2SnZn$ motifs.
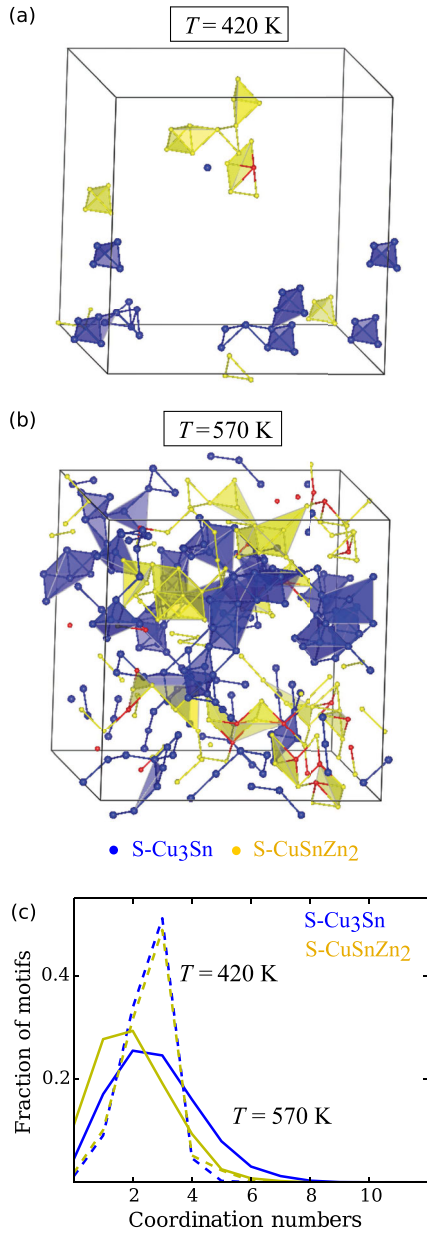
(a)

(b)

FIG. 5. Clustering of motifs in Cu_2SnZnS_4 (CZTS). (a),(b) Distribution of S-Cu_3Sn (blue) and S-$CuSnZn_2$ (yellow) motifs in CZTS at 420 K (b) and 570 K (c). For clarity, the S-Cu_2SnZn motifs are omitted. (c) Distribution of coordination numbers for S-Cu_3Sn (blue) and S-$CuSnZn_2$ (yellow) motifs at 420 K (dashed line) and 570 K (solid line).

occur in triples and quadruplets rather than being dispersed as single unconnected motifs [Figs. 5(a) and 5(c)], which one would expect from entropy considerations at low concentrations if the motifs were independent entities. As the number of S-Cu_3Sn motifs increases, the clusters grow in size and form nanometer-scale inhomogeneities [cf. Figs. 5(b) and 5(c)]. As a result, disproportionation of S-Cu_2SnZn motifs leads to formation of Cu-rich–Zn-poor and Cu-poor–Zn-rich regions in CZTS.

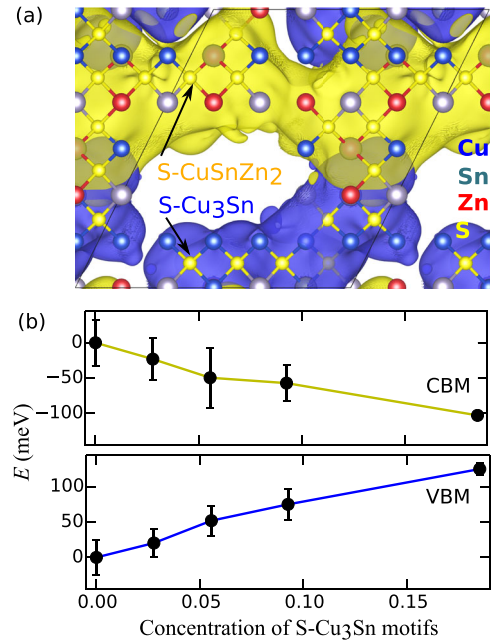FIG. 6. Effects of formation and clustering of S-Cu_3Sn and S-$CuSnZn_2$ motifs in CZTS, as obtained from Monte Carlo simulations. (a) Difference between the electrostatic potentials between ordered CZTS (kesterite) and disordered CZTS (kesterite with 10% concentration of S-Cu_3Sn motifs, which corresponds to the temperature $T_c = 470$ K); yellow (blue) isosurfaces indicate positive (negative) potential difference at 200 meV. For clarity, S-$CuSnZn_2$ motifs are omitted. (b) Change in the position of the valence- and conduction-band edges as a function the concentration of S-Cu_3Sn motifs in CZTS.

C. Consequences of clustering

The presence of structurally coherent compositional inhomogeneities in solar-absorber materials may have important consequences for PV applications. In Fig. 6(a), we show the isosurface of the change of the electrostatic potential due to the disproportionation of 10% of the S-Cu_2SnZn motifs into S-Cu_3Sn and S-$CuSnZn_2$ which corresponds to the temperature $T_c = 470$ K. The disproportionation and clustering of motifs in CZTS leads to strong spatial electrostatic potential fluctuations with the positive amplitude localized around S-Cu_3Sn motifs (Cu-rich–Zn-poor regions) and negative around S-$CuSnZn_2$ motifs (Cu-poor–Zn-rich regions). These fluctuations lead to band tailing and an overall band-gap narrowing [cf. Fig. 6(b)]. Cu-rich S-Cu_3Sn motifs raise the valence-band maximum because of the increased overlap between $Cu(d)$ states and/or the negative electrostatic potential acting on the $Cu(d)$ and $S(p)$ states that built the valence band, whereas Zn-rich S-$CuSnZn_2$ motifs lower the conduction band because of the positive electrostatic potential acting on conduction-band $Sn(s)$ and $S(p)$ states. As discussed in the introduction, band-gap and electrostatic potential fluctuations can be detrimental to the open-circuit voltage of PV devices [5,18].

Importantly, cation disorder and clustering may not only result from high-temperature growth conditions, where entropy dominates the Helmholtz free energy, but also can arise due to nonequilibrium growth conditions at low temperatures [37,38]. For example, in the case of CTS growth, the cubic disordered phase is observed not only above the cubic phase-transition temperature, but also at lower temperatures when it should be partially ordered tetragonal or fully ordered monoclinic [25].

Finally, we note that while the formation of compositional inhomogeneities can be detrimental for PV absorbers, it may be beneficial for thermoelectric materials. Thermoelectric efficiency depends on the dimensionless figure of merit $ZT = \sigma S^2 T/\kappa$, where σ is the electrical conductivity, S is the Seebeck coefficient, T is temperature, and κ is the thermal conductivity. The presence of compositional inhomogeneities may increase the Seebeck coefficient through an energy-filtering effect: Band-gap and electrostatic potential fluctuations can lead to scattering of low-energy carriers and increase asymmetry in differential conductivity [39]. Compositional inhomogeneities can also reduce thermal conductivity [40] and lead to higher electrical conductivity and carrier concentration due to lowering of defect-formation energy [25]. These effects increase the figure of merit ZT and therefore are beneficial to the efficiency of thermoelectric energy conversion.

V. CONCLUSIONS

We demonstrate the possibility of entropy-driven formation of compositional inhomogeneities in tetrahedrally bonded solar absorbers. In CTS, such inhomogeneities form due to entropy-driven segregation of S-Cu_2Sn_2 and S-Cu_3Sn motifs that are building blocks of the ground-state CTS structure. Formation of other motifs in this material is energetically unfavorable because they significantly violate the octet rule. CZTS, on the other hand, consists of a single S-Cu_2SnZn building block, which means that disorder-induced compositional inhomogeneities do not occur unless non-ground-state motifs are created. In this material, however, the formation of other motifs requires less energy, leading to a transition from a single-motif to a multimotif phase at ~470 K. This transition is dominated by the disproportionation of S-Cu_2SnZn into S-Cu_3Sn and S-$CuSnZn_2$ motifs. The subsequent clustering of S-Cu_3Sn and S-$CuSnZn_2$ motifs leads to the formation of (sub-) nanometer-scale compositional inhomogeneities, causing both electrostatic potential and band-gap fluctuations, which are detrimental for photovoltaic applications.

The motif-based model of this work can serve to quantify the propensity of multinary semiconductors that are formed by elemental substitution on a given crystal lattice, such as the zinc-blende structure [21]. For solar cells, materials are desirable that have a single-motif ground state, and a high-energy threshold for formation

of non-native motifs. While these conditions are trivially satisfied for binary materials such as CdTe, they should also be met for the single-motif ternary materials such as $CuInSe_2$ or Cu_3SbS_4, where formation of non-ground-state motifs leads to larger violation of the octet rule than in CZTS. Finally, we note that, while entropy-driven clustering is detrimental for PV absorbers, it could be beneficial for thermoelectric applications.

[1] B. G. Mendis, M. D. Shannon, M. C. J. Goodman, J. D. Major, A. A. Taylor, D. P. Halliday, and K. Durose, The nature of electrostatic potential fluctuations in Cu_2ZnSnS_4 and their role on photovoltaic device performance, J. Phys. Conf. Ser. **471**, 012014 (2013).

[2] M. Dimitrievska, A. Fairbrother, X. Fontané, T. Jawhari, V. Izquierdo-Roca, E. Saucedo, and A. Pérez-Rodríguez, Multiwavelength excitation Raman scattering study of polycrystalline kesterite Cu_2ZnSnS_4 thin films, Appl. Phys. Lett. **104**, 021901 (2014).

[3] B. I. Shklovskii and A. L. Efros, *Electronic Properties of Doped Semiconductor* (Springer-Verlag, Berlin, 1984).

[4] M. A. Krivoglaz, Fluctuon states of electrons, Sov. Phys. Usp. **16**, 856 (1974).

[5] J. H. Werner, J. Mattheis, and U. Rau, Efficiency limitations of polycrystalline thin film solar cells: Case of $Cu(In, Ga)Se_2$, Thin Solid Films **480–481**, 399 (2005).

[6] J. J. S. Scragg, L. Choubrac, A. Lafond, T. Ericson, and C. Platzer-Björkman, A low-temperature order-disorder transition in Cu_2ZnSnS_4 thin films, Appl. Phys. Lett. **104**, 041911 (2014).

[7] A. Khare, B. Himmetoglu, M. Johnson, D. J. Norris, M. Cococcioni, and E. S. Aydil, Calculation of the lattice dynamics and Raman spectra of copper zinc tin chalcogenides and comparison to experiments, J. Appl. Phys. **111**, 083707 (2012).

[8] A. Lafond, L. Choubrac, C. Guillot-Deudon, P. Fertey, M. Evain, and S. Jobic, X-ray resonant single-crystal diffraction technique: A powerful tool to investigate the kesterite structure of the photovoltaic Cu_2ZnSnS_4 compound, Acta Crystallogr. Sect. B **70**, 390 (2014).

[9] T. Washio, H. Nozaki, T. Fukano, T. Motohiro, K. Jimbo, and H. Katagiri, Analysis of lattice site occupancy in kesterite structure of Cu_2ZnSnS_4 films using synchrotron radiation x-ray diffraction, J. Appl. Phys. **110**, 074511 (2011).

[10] M. J. Romero, H. Du, G. Teeter, Y. Yan, and M. M. Al-Jassim, Comparative study of the luminescence and intrinsic point defects in the kesterite Cu_2ZnSnS_4 and chalcopyrite $Cu(In, Ga)Se_2$ thin films used in photovoltaic applications, Phys. Rev. B **84**, 165324 (2011).

[11] E. Zillner, A. Paul, J. Jutimoosik, S. Chandarak, T. Monnor, S. Rujirawat, R.Yimnirun, X. Z. Lin, A. Ennaoui, T. Dittrich, and M. Lux-Steiner, Lattice positions of Sn in Cu_2ZnSnS_4 nanoparticles and thin films studied by synchrotron x-ray absorption near edge structure analysis, Appl. Phys. Lett. **102**, 221908 (2013).

[12] L. Choubrac, M. Paris, A. Lafond, C. Guillot-Deudon, X. Rocquefelte, and S. Jobic, Multinuclear (^{67}Zn, ^{119}Sn and ^{65}Cu) NMR spectroscopy: An ideal technique to probe the cationic ordering in Cu_2ZnSnS_4 photovoltaic materials, Phys. Chem. Chem. Phys. **15**, 10722 (2013).

[13] S. Schorr, The crystal structure of kesterite type compounds: A neutron and x-ray diffraction study, Sol. Energy Mater. Sol. Cells **95**, 1482 (2011).

[14] B. G. Mendis, M. D. Shannon, M. C. J. Goodman, J. D. Major, R. Claridge, D. P. Halliday, and K. Durose, Direct observation of Cu, Zn cation disorder in Cu_2ZnSnS_4 solar cell absorber material using aberration corrected scanning transmission electron microscopy, Prog. Photovoltaics **22**, 24 (2014).

[15] T. Gershon, B. Shin, T. Gokmen, S. Lu, N. Bojarczuk, and S. Guha, Relationship between Cu_2ZnSnS_4 quasi donor-acceptor pair density and solar cell efficiency, Appl. Phys. Lett. **103**, 193903 (2013).

[16] S. Levcenko, V. E. Tezlevan, E. Arushanov, S. Schorr, and T. Unold, Free-to-bound recombination in near stoichiometric Cu_2ZnSnS_4 single crystals, Phys. Rev. B **86**, 045206 (2012).

[17] X. Fontané, V. Izquierdo-Roca, E. Saucedo, S. Schorr, V. O. Yukhymchuk, M. Y. Valakh, A. Pérez-Rodríguez, and J. R. Morante, Vibrational properties of stannite and kesterite type compounds: Raman scattering analysis of $Cu_2(Fe, Zn)SnS_4$, J. Alloys Compd. **539**, 190 (2012).

[18] T. Gokmen, O. Gunawan, T. K. Todorov, and D. B. Mitzi, Band tailing and efficiency limitation in kesterite solar cells, Appl. Phys. Lett. **103**, 103506 (2013).

[19] N. Feldberg, J. D. Aldous, W. M. Linhart, L. J. Phillips, K. Durose, P. A. Stampe, R. J. Kennedy, D. O. Scanlon, G. Vardar, R. L. Field III, T. Y. Jen, R. S. Goldman, T. D. Veal, and S. M. Durbin, Growth, disorder, and physical properties of $ZnSnN_2$, Appl. Phys. Lett. **103**, 042109 (2013).

[20] J. van Embden, K. Latham, and Y. Tachibana, Near-infrared absorbing $Cu_{12}Sb_4S_{13}$ and Cu_3SbS_4 nanocrystals: Synthesis, characterization, and photoelectrochemistry, J. Am. Chem. Soc. **135**, 11562 (2013).

[21] S. Chen, X. G. Gong, A. Walsh, and S. Wei, Electronic structure and stability of quaternary chalcogenide semiconductors derived from cation cross-substitution of II–VI and I–III VI_2 compounds, Phys. Rev. B **79**, 165211 (2009).

[22] S. Delbos, Kësterite thin films for photovoltaics: A review, EPJ Photovoltaics **3**, 35004 (2012).

[23] P. A. Fernandes, P. M. P. Salome, and A. F. da Cunha, Cu_xSnS_{x+1} ($x = 2, 3$) thin films grown by sulfurization of metallic precursors deposited by dc magnetron sputtering, Phys. Status Solidi **7**, 901 (2010).

[24] P. Zawadzki, L. L. Baranowski, H. Peng, E. S. Toberer, D. S. Ginley, W. Tumas, S. Lany, and A. Zakutayev, Evaluation of photovoltaic materials within the Cu-Sn-S family, Appl. Phys. Lett. **103**, 253902 (2013).

[25] L. Baranowski, P. P. Zawadzki, S. T. Christensen, D. Nordlund, S. Lany, A. C. Tamboli, L. Gedvilas, D. S. Ginley, W. Tumas, E. S. Toberer, and A. Zakutayev, Control of doping in Cu_2SnS_3 through defects and alloying, Chem. Mater. **26**, 4951 (2014).

[26] S. Schorr and G. Gonzalez-Aviles, *In-situ* investigation of the structural phase transition in kesterite, Phys. Status Solidi A **206**, 1054 (2009).

[27] J. M. Sanchez and D. de Fontaine, *Structure and Bonding in Crystals* (Academic, New York, 1981), p. 117.

[28] C. Wolverton and D. de Fontaine, Cluster expansions of alloy energetics in ternary intermetallics, Phys. Rev. B **49**, 8627 (1994).

[29] S. L. Dudarev, G. A. Botton, S. Y. Savrasov, C. J. Humphreys, and A. P. Sutton, Electron-energy-loss spectra and the structural stability of nickel oxide: An LSDA + U study, Phys. Rev. B **57**, 1505 (1998).

[30] J. P. Perdew, K. Burke, and M. Ernzerhof, Generalized Gradient Approximation Made Simple, Phys. Rev. Lett. **77**, 3865 (1996); Generalized Gradient Approximation Made Simple, **78**, 1396 (1997).

[31] G. Kresse and J. Furthmüller, Efficient iterative schemes for *ab initio* total-energy calculations using a plane-wave basis set, Phys. Rev. B **54**, 11169 (1996).

[32] V. Stevanović, S. Lany, X. Zhang, and A. Zunger, Correcting density functional theory for accurate predictions of compound enthalpies of formation: Fitted elemental-phase reference energies, Phys. Rev. B **85**, 115104 (2012).

[33] T. Poggio, R. Rifkin, S. Mukherjee, and P. Niyogi, General conditions for predictivity in learning theory, Nature (London) **428**, 419 (2004).

[34] S. Asakura and F. Oosawa, On interaction between two bodies immersed in a solution of macromolecules, J. Chem. Phys. **22**, 1255 (1954).

[35] D. Huang and C. Persson, Band gap change induced by defect complexes in Cu_2ZnSnS_4, Thin Solid Films **535**, 265 (2013).

[36] A. Walsh, S. Chen, S.-H. Wei, and X.-G. Gong, Kesterite thin-film solar cells: Advances in materials modelling of Cu_2ZnSnS_4, Adv. Energy Mater. **2**, 400 (2012).

[37] P. Zawadzki, J. Perkins, and S. Lany, Modeling amorphous thin films: Kinetically limited minimization, Phys. Rev. B **90**, 094203 (2014).

[38] P. F. Ndione, Y. Shi, V. Stevanovic, S. Lany, A. Zakutayev, P. A. Parilla, J. D. Perkins, J. J. Berry, D. S. Ginley, and M. F. Toney, Control of the electrical properties in spinel oxides by manipulating the cation disorder, Adv. Funct. Mater. **24**, 610 (2014).

[39] J. Bahk, Z. Bian, and A. Shakouri, Electron energy filtering by a nonplanar potential to enhance the thermoelectric power factor in bulk materials, Phys. Rev. B **87**, 075204 (2013).

[40] J. Androulakis, C.-H. Lin, H.-J. Kong, C. Uher, C.-I. Wu, T. Hogan, B. A. Cook, T. Caillat, K. M. Paraskevopoulos, and M. G. Kanatzidis, Spinodal decomposition and nucleation and growth as a means to bulk nanostructured thermoelectrics: enhanced performance in $Pb(1 − x)Sn(x)Te − PbS$, J. Am. Chem. Soc. **129**, 9780 (2007).